



**HAL**  
open science

# 1D strain rate-dependent constitutive model of UHMWPE: From crystalline network to fibrillar structure behavior

Tiana Deplancke, Fivel Marc, Olivier Lame

► **To cite this version:**

Tiana Deplancke, Fivel Marc, Olivier Lame. 1D strain rate-dependent constitutive model of UHMWPE: From crystalline network to fibrillar structure behavior. *Mechanics of Materials*, 2019, 137, pp.103129. 10.1016/j.mechmat.2019.103129 . hal-02270638

**HAL Id: hal-02270638**

**<https://hal.science/hal-02270638>**

Submitted on 22 Dec 2020

**HAL** is a multi-disciplinary open access archive for the deposit and dissemination of scientific research documents, whether they are published or not. The documents may come from teaching and research institutions in France or abroad, or from public or private research centers.

L'archive ouverte pluridisciplinaire **HAL**, est destinée au dépôt et à la diffusion de documents scientifiques de niveau recherche, publiés ou non, émanant des établissements d'enseignement et de recherche français ou étrangers, des laboratoires publics ou privés.

# 1D strain rate-dependent constitutive model of UHMWPE: from crystalline network to fibrillar structure behavior

Tiana Deplancke<sup>1</sup>, Marc Fivel<sup>1</sup>, Olivier Lame<sup>2</sup>

<sup>1</sup>Univ. Grenoble Alpes, CNRS, SIMaP, F-38000 Grenoble, France

<sup>2</sup>Université de Lyon, CNRS, INSA-Lyon, MATEIS, UMR5510, F-69621, Villeurbanne, France

## **ABSTRACT**

A combined experimental and analytical investigation has been performed to understand and predict the mechanical behavior of UHMWPE with different molecular weights: 0.6; 3.9 and 10.5 Million g/mol. These materials were tested to a wide range of strain rates using uniaxial compression tests on a servo-hydraulic testing machine for the lowest strain rates ( $10^{-4}$  to  $10$  s<sup>-1</sup>) and magnesium split Hopkinson pressure bars for the highest strain rates ( $10^3$  s<sup>-1</sup>).

A hyperelastic-viscoplastic approach based on a relevant physical basis was adopted to predict the mechanical behavior of UHMWPE. The key point of the proposed model is to capture the huge microstructural evolution which occurs during fibrillation (crystalline network collapse) through a mechanical coupling parameter between the confined amorphous phase and the crystal stacks. The description of the amorphous phase is split in two parts, confined and global macromolecular networks in order to account for experimental results such as the huge strain recovery observed even after large plastic deformation of UHMWPE.

It is found that this model successfully describes the compressive hyperelastic-viscoplastic behavior of sintered UHMWPE for different molecular weights over a wide range of strain rates and can be qualitatively extended to tensile and cyclic loadings.

**Keywords:** constitutive behavior, semicrystalline polymeric material, mechanical testing, microstructures, UHMWPE

## 1. INTRODUCTION

The mechanical behavior of semicrystalline polymers is highly non-linear and sensitive to several external parameters (such as temperature, strain rate) and structural factors (crystallinity, molecular weight, physical entanglements and cross-linking). Semicrystalline polymers may be considered as nano-composite materials. Their structure comprises both amorphous and crystalline phases interconnected in a complex manner.

Over the past two decades several constitutive models were proposed to capture the hyperelastic-viscoplastic deformation behavior of solid polymers. Because of the complexity of the problem and due to the lack of a detailed understanding of the local deformation mechanisms, several authors developed phenomenological models (Bardenhagen et al., 1997; Epee et al., 2011; Khan and Zhang, 2001; Krairi and Doghri, 2014; Pouriayevali et al., 2013; Yakimets et al., 2007).

In the case of amorphous polymers, both glassy and rubbery states have been taken into account in physically based models that gave rather satisfactory and predictive results. They are often inspired by the early work of Haward and Thackray (Boyce and Arruda, 2000; Buckley and Jones, 1995; Haward and Thackray, 1968; Xue et al., 1998). More recently, mechanical modeling connecting both yielding and strain hardening (due to the evolution of the macromolecular network

structure) have been also proposed (Haward, 1993; Senden et al., 2010). When considering the semicrystalline polymer both phenomenological (Ayoub et al., 2010; Drozdov, 2009; Dusunceli and Colak, 2008; Khan et al., 2006; Maurel-Pantel et al., 2015; Regrain et al., 2009) and micro-macro approaches have been proposed (Dommelen et al., 2003; Gueguen et al., 2010; Nikolov et al., 2002; Sedighiamiri et al., 2014; Shojaei and Li, 2013; Uchida et al., 2010).

All these approaches can be accurate in a certain domain, but their main drawback is that they cannot really capture the huge microstructural evolution that occurs during fibrillation of a semicrystalline polymer. As a consequence, their reliability beyond their fitted domain remains limited.

On the other hand, physical approaches (generally 1D models) that have been developed since the 70s have allowed establishing the main deformation mechanisms that occur during the elastic regime, the fibrillation stage and the fracture process. Viscoelasticity, plasticity, damage, hardening and fibrillation fractures with crack propagation are qualitatively well described in the literature (Bouvard et al., 2009; Michler and Baltá-Calleja, 2016; Ward and Sweeney, 2001).

Since macroscopic approaches do not take into account the huge microstructural evolution occurring during fibrillation (crystalline network collapse), plasticity is generally viewed as a continuous process from yielding to hardening. This is one of the main weak points of semi crystalline modeling that should be addressed in a physical approach as the mechanisms of fibrillation are qualitatively well understood, and can accurately reproduce a memory effect between the initial and fibrillar structure (Xiong et al., 2016). Basically, plastic flow leads to strong softening due to fractures of crystalline lamellae into small blocks. However, entanglements and molecular intercrystalline connections progressively catch up this collapse leading finally to hardening. It is largely agreed that these connections are essentially contained in the confined

amorphous phase and behaves as Stress Transmitters (ST see (Seguela, 2005)). They are supposed to be essentially composed of chains connecting adjacent crystallites, namely, Tie Molecules (TMs) which are known to strongly affect the mechanical properties of semicrystalline polymers both in the elastic domain as well as during the plastic behavior. Their direct quantification remains however impossible. According to the work of Huang et al. (Huang and Brown, 1991), the probability of forming a tie molecule increases with the molecular mass of the polymer. As a consequence, it exists a critical molecular weight above which chains becomes intertwined into a macromolecular network (Huang and Brown, 1991; Porter and Johnson, 1966; Seguela, 2005). Some modeling approaches have been proposed to establish connections between the macroscopic mechanical behavior and this specific amorphous phase (G'sell and Dahoun, 1994; Lee et al., 1993; Oshmyan et al., 2004; Roguet et al., 2007).

In the case of Ultra High Molecular Weight Polyethylene (UHMWPE), the length of the chains implies that nearly all the chains are tie chains, and this asserts a very strong macromolecular network that is generally used to explain the unusual capabilities to accumulate deformation without necking (Bonten and Schmachtenberg, 2001; Humbert et al., 2009). Very few attempts exist for modeling the mechanical behavior of such a polymer (Bergström et al., 2002), and microstructural specific features are not explicitly taken into account. The strong macromolecular network should clearly be included in a realistic mechanical constitutive law.

UHMWPE is also known to exhibit exceptional wear and impact resistance. As an example, a recent study has highlighted the outstanding shock resistance of UHMWPE in the case of hydrodynamic cavitation erosion (Deplancke et al., 2015a). However, it remains very difficult to predict the plastic deformation and the life time of the coatings under such severe conditions and

thus numerical modeling is required. This implies to set up an accurate model of elasto-viscoplastic behavior of UHMWPE capable to take care of large strain rates.

This paper presents a mixt approach of the mechanical behavior of UHMWPE combining experimental investigations of sintered UHMWPE with various molecular weights under high strain rate (comparable to impact induced by cavitation erosion) and numerical modeling of the same materials for a large range of strain rates.

To predict the behavior of UHMWPE we propose first a general physical approach aiming at describing the mechanical behavior of the semicrystalline polymers both in the elastic and plastic regime by including the main physical mechanisms existing in the literature. Then, the model will be adapted to UHMWPE by adjusting some of its parameters, in particular to take into account the huge strain recovery observed on these materials even after a large plastic deformation. Such a model could ultimately be used to explain the resistance to cavitation erosion as supposed to happen at high strain rate (Roy et al., 2015).

## **2. EXPERIMENTAL PART**

### ***2.1. Materials***

The UHMWPE under investigation is elaborated from three different commercial nascent reactor powders produced by Celanese (ex-Ticona, Oberhausen, Germany). Their average molecular weights deduced from viscosity measurements are ranged between  $M_v = 0.6, 3.9$  and  $10.5$  million g/mol (GHR 8110, GUR 4113 and 4170 respectively). This nascent powder was processed by sintering performed in an Instron compressive testing machine equipped with an oven “Servantin”. The sintering protocol was optimized in order to obtain the best mechanical properties (see (Deplancke et al., 2015b, 2014) for details of the protocol).

Cylindrical compression tests specimens with 8 mm in diameter and 8-9 mm in height were then machined out from the sintered samples.

The crystallinity ratio was measured by DSC using a Perkin Elmer Pyris apparatus at a heating rate of 10 °C/min, and calculated considering that the melting enthalpy of a perfect PE crystal is  $H_m^0 = 290 \text{ J/g}$  (Wunderlich, 2003).

## ***2.2. Mechanical characterization***

Compression tests have been performed on the three materials with different molecular weights, at strain rates ranging between  $10^{-4}$  and  $10 \text{ s}^{-1}$  using a conventional servo-hydraulic MTS compression testing apparatus at room temperature with a load cell of 100 kN and compression platens with ball-joint system.

To reduce the friction at the platen/specimen interface, the platens were polished and thin Teflon (PTFE) films were used as lubricating layers between the specimen and the platens.

These compression tests have been complemented by Split Hopkinson Pressure Bar (SHPB) tests for accessing higher strain rates of  $10^3 \text{ s}^{-1}$ . This experimental device is based on wave propagation and the specimen mechanical impedance must be adapted to the bars impedances (Gama et al., 2004). In the case of UHMWPE, 2 m long and 38.2 mm diameter magnesium alloy Mg ZK60 T5 bars have been used. The gas gun is filled with compressed air at a pressure of around 4 bars, which represents a mean strain rate of  $10^3 \text{ s}^{-1}$ . The three-wave technic (Gama et al., 2004) is used to obtain stress strain curves (see (Pfeiffer, 2015) for details of the protocol and device).

Assuming homogeneous deformation of all samples irrespective of drawing conditions, the true strain was computed as  $\epsilon = \ln(L/L_0)$ , where  $L_0$  is the initial sample gauge length and  $L$  its length

under straining. The true stress was defined as  $\sigma = F\lambda / S_0$ , where  $F$  is the tensile force,  $\lambda = L/L_0$  is the draw ratio, and  $S_0$  is the initial sample cross section. This computation assumes isovolumic strain, neglecting Poisson's effect and cavitation.

### 3. RESULTS AND ANALYSIS

The figure 1 displays selected results of compression tests for different strain rates between  $10^{-4}$  and  $10^3 \text{ s}^{-1}$  on the sintered UHMWPE with 3 different molecular weights 0.6, 3.9 and 10.5 Mg/mol. Each true stress-strain curve displayed on these plots is a representative curve averaged among four realizations of independent compressive tests.

These curves show:

- A dispersion of the elastic modulus certainly due to the measurement made without any extensometer. To avoid this problem, the data used for numerical identification will be the average elastic moduli of the four compressive tests, measured between 1 and 3% deformation for each strain rate.
- An increase in yield stress with the strain rate followed by strain hardening. The slope of the strain hardening increase also with the strain rate.
- An immediate recovery, of the order of 20%, is observable during the unload stage which was performed at the same strain rate as the loading part. This immediate recovery is strongly dependent of the molecular weight.

Recovery tests over long periods of time, of the order of the month, display a recovery close to 100% both for the molecular weight of 10.5 Mg/mol and 3.9Mg/mol and 85% for the molecular weight of 0.6 Mg/mol in the case of the strain rates between  $10^{-4} \text{ s}^{-1}$  and  $1 \text{ s}^{-1}$ . Indeed, measurements of specimen dimensions after these compression tests reveal almost no change in shape and a

length equal to the initial length is recovered in the case of the molecular weight of 10.5 Mg/mol after one month of relaxation.

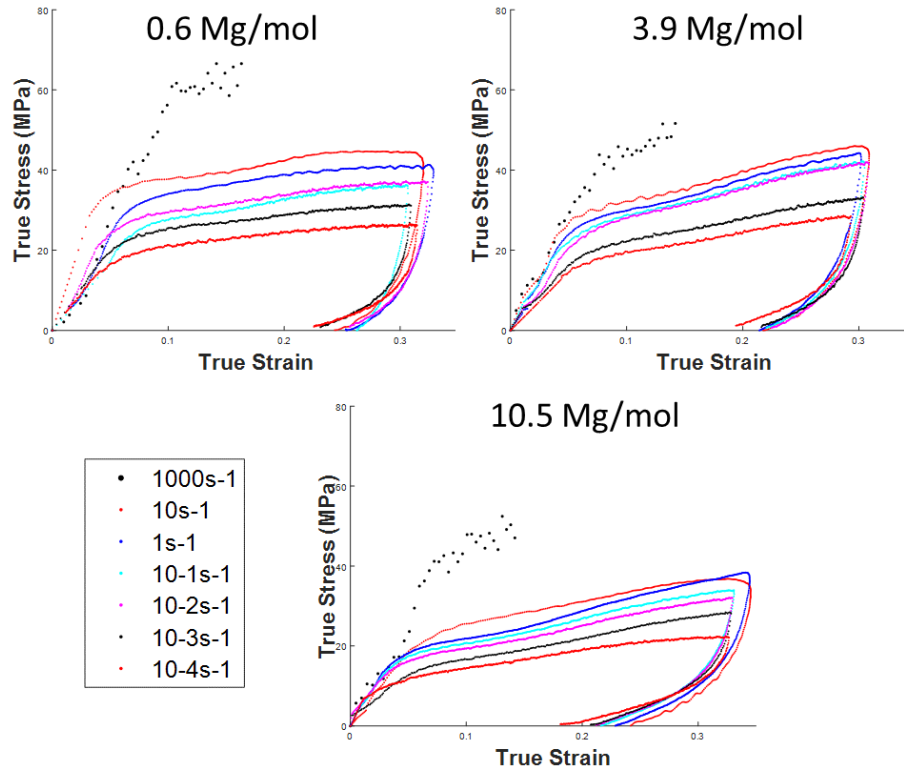


**Figure 1:** Experimental strain-stress curves from compressive tests on the three molecular weights and various strain rates in the range from  $10^{-4} \text{ s}^{-1}$  to  $1000\text{s}^{-1}$ .

Figure 2 shows typical compression tests realized on the sintered UHMWPE for 2 different maximum deformations (40% and 80%) for the molecular weights of 0.6 and 10.5 Mg/mol and at a strain rate of  $0.1 \text{ s}^{-1}$ .

The first striking observation is that the shape of the 'unload part' of the curves are very similar regardless of the maximal deformation.

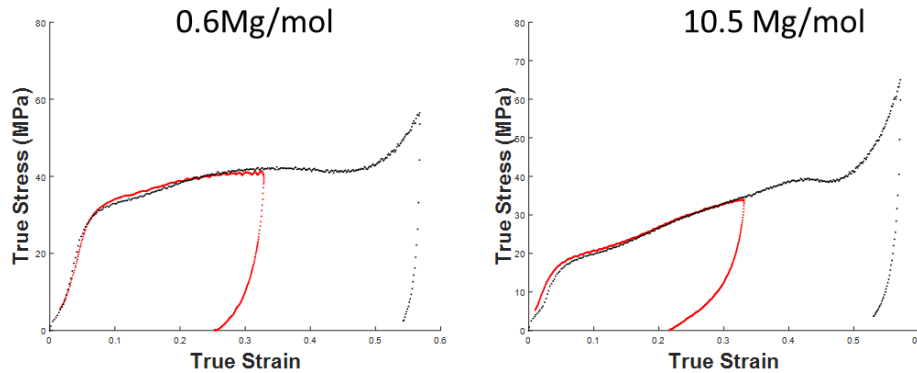


**Figure 2:** Strain-stress curves of the experimental compressive tests for molecular weights 0.6 and 10.5 Mg/mol at strain rate  $0.1\text{s}^{-1}$ .

Observation of the deformed samples show a barreling effect for plastic deformation above 0.5 so that it could explain the change of slope visible on the curves at this cumulated true strain. This artefact comes from the estimation of the true strain based on a non-local measurement of the elongation. We will not consider this change of slope in our modeling.

Consequently, the model presented in this article will take into account the following experimental observations of the mechanical behavior of sintered UHMWPE:

- First a recovery in very short times occurs whatever the speed of deformation and the form of this recovery is very similar for several deformations.
- In addition, one of the specificities of the UHMWPE is that a recovery in longer times (of the order of the month) allows a quasi-complete recovery for deformation as large as 40%.

Therefore, the model proposed in this article should allow to reproduce these two experimental observations and should also remain in agreement with all the observations of the literature concerning the mechanical behavior of the semicrystalline polymers.

#### 4. CONSTITUTIVE MODEL OF UHMWPE

The main purpose of this part is to propose a uniaxial constitutive model able to reproduce (at least semi-quantitatively) the hyperelasto-viscoplastic response of the three UHMWPE materials for various molecular weights between 0.6 and 10.5 Mg/mol over a wide range of strain-rates: from  $10^{-4}$  to  $10^3$  s<sup>-1</sup>. As a uniaxial model, it is relatively easy to include all the physical mechanisms on which there is a consensus in order to i) obtain a model which is satisfactory and understandable from a physical point of view and ii) to promote a better reliability when varying parameters such as the strain rate, crystallinity, etc.

As soon as the crystallinity exceeds a few percent, it is generally admitted that a semicrystalline polymer can be considered as a macromolecular network (a rubber when  $T > T_g$ ) bridled by a crystalline network formed by lamellar stacking (Detrez, F; Séguéla, R.; Cantournet, 2009; Detrez et al., 2011) generally arranged in an isotropic spherulitic structure see figure 3a. It is then reasonable to consider the decomposition of the global stress into two terms corresponding to the two superimposed networks (see figure 3). In the case of medium molecular mass PE, the macromolecular network consists essentially of the confined amorphous phase which can flow relatively easily at high stress. This assumption is close to the one proposed by Ward and Ayoud (Ayoub et al., 2011, 2010; Ward, 1984) and used in several modeling approaches.

In the case of UHMWPE, short range macromolecular network still exists and is even reinforced, but it should also exist a long range macromolecular network that strongly prevents the material from flowing at high stress. Indeed, one should keep in mind that for UHMWPE even after a very high deformation, a nearly full recovery can be observed after several weeks.

As a consequence, we propose first to decompose the stress in two parts: the macromolecular network and the crystalline stack network. The first is strongly involved in the hardening even at

low strain and, of course, the long-term strain recovery. It is particularly important for UHMWPE. The second represents what is common to all semicrystalline polymers i.e. the crystalline stack mechanical behavior. It has to be noticed that this part contains the confined amorphous phase, so that this modeling is itself splitted in two different parts.

$$\sigma = \sigma_{crystal\ stack\ network(CrN)} + \sigma_{macromolecular\ network(MN)} \quad (1)$$

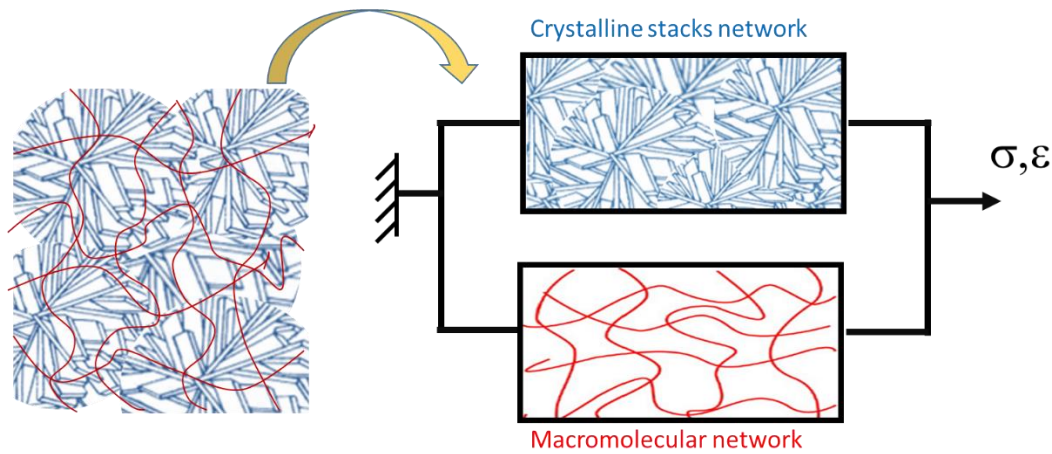


**Figure 3.** Schematic view of (a) the entanglement of crystals and macromolecular network and (b) Rheological model.

For large strain, the crystalline network has collapsed and reorganized into small crystalline blocks that are positioned relatively regularly along a fibril. This collapse induces a large decrease of the material stiffness whereas a progressive mechanical hardening is simultaneously observed. The latter is due to the strong alignment of the chains. Indeed, for a large strain, the macromolecular network is strongly stretched which compensates for the loss of mechanical properties of the crystalline network (see figure 4).

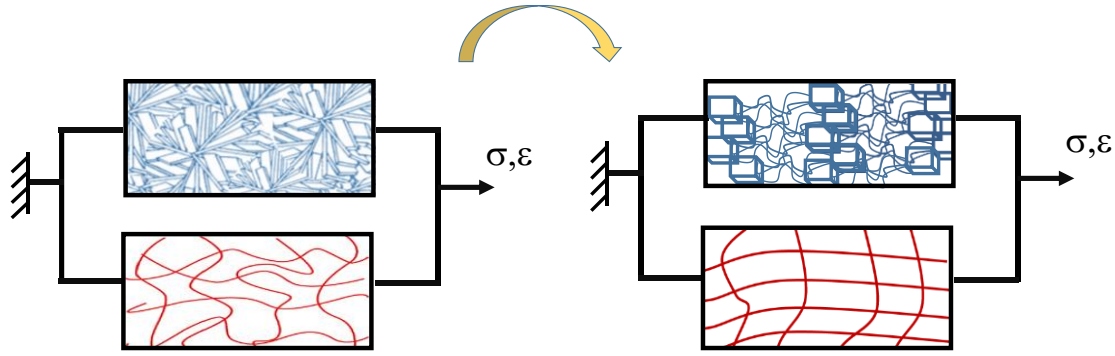


**Figure 4.** Schematic view of the evolution of rheological model for large strain (fibrillation and stretched macromolecular network).

#### 4.1. Description of the macromolecular network branch

In order to model the stretching of the macromolecular network within the strain-hardening stage, the eight-chain network model, developed by Arruda and Boyce (Arruda and Boyce, 1993) is selected for its physical consistency.

$$\sigma_{MN} = C_0 \left( \lambda_{MN}^2 - 1/\lambda_{MN} \right) = \frac{\mu_{MN}}{3} \frac{\sqrt{N_{MN}}}{\lambda_{chainMN}} \mathcal{L}^{-1} \left( \frac{\lambda_{chainMN}}{\sqrt{N_{MN}}} \right) \left( \lambda_{MN}^2 - 1/\lambda_{MN} \right) \quad (2)$$

In equation (2),  $\lambda_{MN} = \varepsilon_{MN} + 1$  is the draw ratio of the macromolecular network,

$$\lambda_{chainMN} = \frac{\sqrt{\lambda_{MN}^2 - 2/\lambda_{MN}}}{\sqrt{3}}$$

is the stretch of a chain in the eight-chain network in the case of one-

dimensional mechanical testing,  $\mathcal{L}^{-1}$  is the inverse Langevin function,  $\sqrt{N_{MN}}$  the limiting chain extensibility of the macromolecular network and  $\mu_M$  the rubbery modulus.

This model however does not capture the increase of the strain-hardening modulus, with the strain rate. Following the work of Govaert and Haward (Goveart et al., 2008; Haward, 1993; Senden et al., 2010), a viscous contribution is added to the entropic elasticity. This flow stress is related to the intermolecular frictions at a monomeric or segmental scale. The viscous flow stress is a

function of the strain rate  $\dot{\varepsilon}$ , which is described by an Eyring relation expressed as a function of the total deformation:

$$C_{app}(\dot{\varepsilon}) = \frac{k_B T}{\alpha_{MN}} \sinh^{-1} \left( \frac{\dot{\varepsilon} h}{k_B T} \exp\left(\frac{\Delta H_{MN}}{k_B T}\right) \right) \quad (3)$$

With  $\dot{\varepsilon}$  the strain rate,  $\Delta H_M$  the activation energy and  $\alpha_M$  the activation volume.

Therefore, the elastic stress in uniaxial loading is represented by the following relation:

$$\sigma_{MN} = (C_0 + C_{app}(\dot{\varepsilon})) \left( \lambda_{MN}^2 - 1 / \lambda_{MN} \right) \quad (4)$$

where  $C_0$  is the Boyce modulus,  $C_{app}$  is the viscous contribution of the strain hardening and  $\lambda_{MN} = \varepsilon + 1$  is the draw ratio of the macromolecular network.

A similar elastic model has been successfully applied to semicrystalline polymers (Haward, 1993) and it was able to capture the essential of the physics of the hardening behavior. The model can be schematically represented by two springs, one is strain rate dependent whereas the second is not (see fig 5).

A viscous dashpot is added in series to the macromolecular network description in order to allow for possible creep of the macromolecular network since the chains are not cross-linked, and ultimately to describe the damage by viscous flow. The mechanism associated with the flow could be chains fractures or reptation activated by the stress.

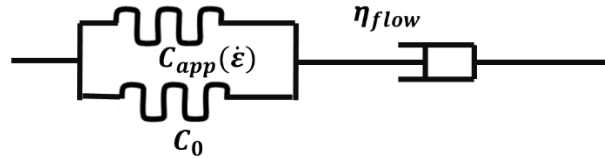


**Figure 5.** Rheological representation of the part "Macromolecular Network" of the constitutive model.

However, even in the region of very large strain, this phenomenon should be weak for most of the UHMWPE when the temperature remains below the melting point. Thus, the flow behavior of the

macromolecular network is described by a viscosity proportional to the cubic power of the molecular weight as already proposed by Doi and Edwards, 1988 and Wang and Porter, 1995) :

$$\eta_{flow} = G_{flow} M^3 \quad (5)$$

where  $M$  is the molecular weight and  $\eta_{flow}$  the viscosity of the macromolecular network.

Consequently, the plastic deformation of the macromolecular network is given by:

$$\dot{\epsilon}_{flow} = \frac{\sigma_{MN}}{\eta_{flow}} \quad (6)$$

For most of the UHMWPE,  $M$  being huge, this viscosity can be considered (in a first approach) as infinite.

#### ***4.2. Description of the Crystalline network branch***

Two springs, relative to crystalline and confined amorphous parts are used to represent the initial modulus of the material. A simple analytical model with an adjustable mechanical coupling is used to take into account the fact that these two phases are neither in parallel nor in series but rather a mixture of both as expressed in equation (7):

$$\begin{aligned} \sigma_{CrN} &= \varphi \sigma_{cr} + (1 - \varphi) \sigma_{confined\ amorphous\ phase(CA)} \\ &= (1 - \varphi + k\varphi) \sigma_{CA}. \end{aligned} \quad (7)$$

where  $\varphi$  is the crystallinity obtained by DSC experiments and  $k = \sigma_{cr}/\sigma_{CA}$  the adjustable mechanical coupling parameter where  $\sigma_{cr}$  and  $\sigma_{CA}$  are respectively the stress in the crystal and in the confined amorphous phase.

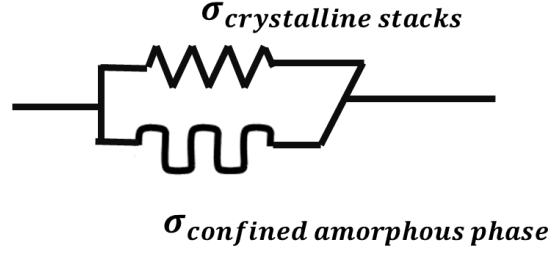


**Figure 6.** Schematic view of the rheological representation of the part "Crystalline stacks network".

The tilted segment in Figure 6 represents this coupling. This model, developed by S.Humbert et al. (Humbert et al., 2011), allowed to capture this dependency for a wide range of polyethylene with different crystallinity and microstructure. A single parameter has to be adjusted. This parameter is the stress ratio parameter  $k = \sigma_{cr}/\sigma_{CA}$  where  $\sigma_{cr}$  and  $\sigma_{CA}$  are respectively the stress in the crystal and in the confined amorphous phase. It represents then the mechanical coupling between the two phases i.e.  $k=1$  corresponds to a series coupling whereas  $k = E_{cr}/E_{CA}$  (where  $E_{cr}$  and  $E_{CA}$  are respectively the modulus in the crystal and confined amorphous phase) leads to a parallel coupling. This model is close to a Halpin Tsai model (Halpin and Kardos, 1976), and is used mainly for the sake of simplicity and because it gives reliable results for medium to high density polyethylene including UHMWPE. It is also suitable to take into account the crystal network collapse occurring during plasticity (see the general description of the constitutive model). The initial value of the parameter  $k$  is fitted on the evolution of the Young's modulus as a function of the crystallinity and it evolves during the plastic deformation of the material. The stress on the crystal network is given by  $\sigma_c = E_c \varepsilon_c$  with  $E_c = 28\text{GPa}$  (Boyd, 1979).

To extrapolate the confined amorphous phase behavior for larger deformation, i.e.during plastic strain, a hyperplastic model has been proposed by (Arruda and Boyce, 1993).

$$\sigma_{CA} = \frac{\mu_{CA}}{3} \frac{\sqrt{N_{CA}}}{\lambda_{chainCA}} \mathcal{L}^{-1} \left( \frac{\lambda_{chainCA}}{\sqrt{N_{CA}}} \right) \left( \lambda_{CA}^2 - 1/\lambda_{CA} \right) \quad (8)$$

In equation (8),  $\lambda_{CA} = \varepsilon_{CA} + 1$  is the draw ratio,  $\lambda_{chainCA} = \frac{\sqrt{\lambda_{CA}^2 - 2}/\lambda_{CA}}{\sqrt{3}}$  is the stretch of a chain in the eight-chain network in the case of one-dimensional mechanical testing,  $\mathcal{L}^{-1}$  is the inverse Langevin function,  $\sqrt{N_{CA}}$  the limiting chain extensibility of the tie molecules which is strongly weaker than that of the rubbery network, and  $\mu_{CA}$  the rubbery modulus.

The amorphous phase confined in the crystallites stacking is not directly comparable to a bulk rubber because of the presence of an interphase, and because they are locked between two crystallites. We have shown that for particular orientations of the stacking, the bulk modulus of the amorphous phase can be more important than the tensile modulus (Xiong et al., 2015). As a consequence, in some cases the apparent tensile modulus of the amorphous phase could be close to 300 MPa. Consequently, the apparent average modulus of the amorphous phase in a semicrystalline polymer has nothing to do with the one of a pure rubber and is much higher. Using our experimental data, an initial value of 70 MPa seems to be appropriate.

Moreover, Tie Molecules (TM) which link adjacent crystallites are also partially responsible for such a high modulus of the amorphous phase (Xiong et al., 2015). Indeed, it has been shown that they are initially taut, explaining why they can affect elastic domain and yielding behavior, as well as fibrillar formation (Men et al., 2003; Seguela, 2005; Xiong et al., 2016) and strain hardening. Similarly to a rubber, these chains can be considered as active chains (Men et al., 2003; Patel et al., 1996; Peterlin, 1967; Seguela, 2005). Due to its entropic elasticity, this network plays a major role in the spring back effect of the material as they still connect the crystalline blocks after fibrillation. Hyper-elastic model is then suitable to describe its behavior considering a very weak limit of extensibility.

### 4.3. Plastic behavior

The plasticity in semicrystalline polymers is known to be due to the motion of dislocations in the crystalline phase which is a thermally activated phenomenon. It is also known that the energy barrier for dislocation motion is increasing with the crystal thickness, and then with the crystallinity.

Based on thermally activated mechanisms and stress driven considerations of defect mobility, the Eyring models (Eyring, 1936; Gueguen et al., 2008; Richeton et al., 2005; Ward, 1984) are classically used to describe the plastic behavior of polymers. For semicrystalline polymers one of the simplest Eyring model can be derived as follows:

$$\dot{\epsilon}_{plastic} = \frac{k_B T}{h} e^{\frac{-\Delta H_{pl}}{k_B T}} / \sinh\left(\frac{\alpha_{pl} \sigma}{k_B T}\right) \quad (9)$$

with  $k_B$  the Boltzmann's constant,  $T$  the temperature (here equal to the room temperature 293 K),  $h$  the Planck constant. Parameters  $\Delta H_{pl}$  and  $\alpha_{pl}$ , correspond respectively to the activation energy and the activation volume and could be dependent on the crystallinity. This model explicitly predicts an increase in the yield stress with the increase of the strain rate.

During plastic deformation, following the Peterlin scheme (Bartczak and Galeski, 2010; Peterlin, 1975, 1967), the microstructure evolves from spherulitic organization where the crystal network is percolating toward a fibrillar microstructure where crystalline blocks are nearly isolated and embedded in the amorphous phase. During this process, the stress concentration in the crystal phase decreases. As a consequence, the mechanical coupling  $k$  in eq.7 evolves from the initial situation where it is intermediate between series and parallel toward a situation where the coupling can be assumed to be close to a series coupling i.e.  $k = 1$ . The fibrillar structure is supposed to be

achieved for a deformation associated to the natural draw ratio (Gent and Madan, 1989; Peterlin, 1987; Seguela, 2007; Ward, 1984).

As a consequence, we propose a strong connection between  $\varepsilon_{\text{plastic}}$  and  $k$  in the crystalline network branch. The following empirical equation is proposed to describe a progressive collapse of the crystalline network as the plastic deformation increases:

$$k = k_{\text{init}} e^{\frac{-\varepsilon_{\text{pl}}}{\varepsilon_{\text{Nat\_Cr}} \text{Ln } k_{\text{init}}}} \quad (10)$$

Where  $k_{\text{init}}$  is determined by fitting a wide range of polyethylene with varying their crystallinity (Humbert et al., 2011),  $\varepsilon_{\text{pl}}$  is determined from Eyring's expression (eq 3), and  $\varepsilon_{\text{Nat\_Cr}}$  is the deformation for which the fibrillar state is reached (corresponding to the series coupling and consequently  $k=1$ ).

In other words, when the fibrillary state is attained, the rheological model of the crystal branch transforms into the series model as shown in the following scheme (fig 7).

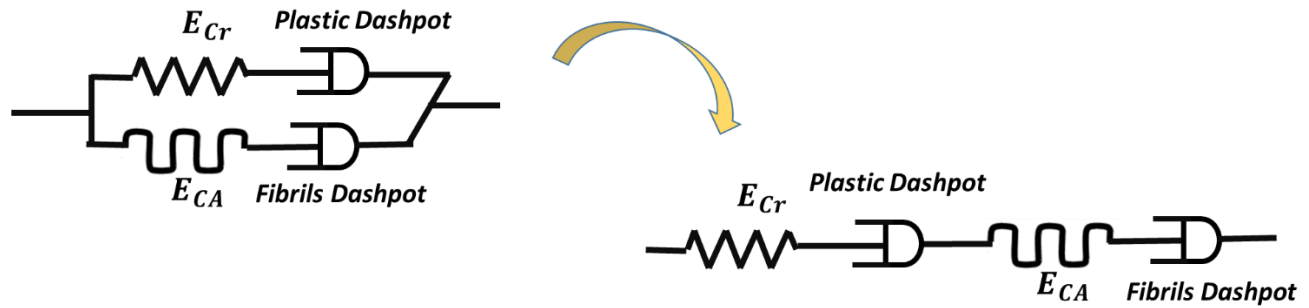


**Figure 7.** Rheological representation of the part "Crystalline stacks network" of the constitutive model and the evolution during stretching.

The form of this equation remains phenomenological, but could be justified for low and medium density polyethylene where the first breakages in the crystalline network are not critical, leading finally to a progressively accelerated decrease of parameter  $k$ .

At larger deformation, it has been experimentally observed that secondary plasticity could occur in the necked region and could even lead to a second necking formation. This plasticity is associated with the slipping of the fibrils or break of the tie molecule and/or partial disentanglement. It could also be unfolding mechanisms or chains pull out (Castagnet et al., 2000) in the crystal blocks.

To capture this plasticity a second non-linear dashpot is added in a series coupling with the spring representative of the confined amorphous phase using the following Eyring model:

$$\dot{\epsilon}_{plastic\_Fibril} = \frac{k_B T}{h} e^{\frac{-\Delta H_{Fibril}}{k_B T}} / \sinh\left(\frac{\alpha_{Fibril} \sigma}{k_B T}\right) \quad (11)$$

The activation barrier of this secondary plasticity should be higher than that of the initial plasticity since it always occurs at higher stress level.

Finally, the behavior of the crystalline network branch is elastic then plastic with a strong softening due to the progressive collapse of the crystalline network. However, the overall behavior of the material does not exhibit softening but hardening.

As a consequence, it means that the second branch (consisting of the macromolecular network) and partially the hardening of the confined amorphous phase, takes over on the crystalline network providing a strong hardening that balances the loss of stress due to the crystalline branch. Note that a similar idea was qualitatively proposed by Peterlin (Peterlin, 1975).

#### ***4.4. Numerical identification of the model parameters***

Following the physical considerations described above, we finally need to solve a two-body system explicitly defined by the following equations:

$$\sigma = \sigma_{crystal\ stack\ network} + \sigma_{macromolecular\ network} \quad (12)$$

with  $\sigma_{crystal\ stack\ network}$  defined by equations 7-11 and  $\sigma_{macromolecular\ network}$  defined by equations 2-6.

Numerically, the time integration of variables  $\varepsilon_{Pl}$  (eq.9),  $\varepsilon_{Pl\_Fibril}$  (eq.11) and  $\varepsilon_{flow}$  (eq.6) is performed using an order two Runge-Kutta scheme.

The overall deformation of the semicrystalline polymer could be separated in several steps associated with different physical parameters such as crystallinity and entanglement network. The numerical identification of the parameters has been thus separated in three steps.

To take into account the dispersion of experimental results, the parameter identification was made with target values corresponding to the stress at selected deformations: eight values per strain rate. Each of these values is an average obtained from the four compressive strain-stress curves for each strain rate.

In the first step, the Young's modulus (describing the crystal network contribution) has been determined by a large set of polyethylene with various crystallinity. Here we use the combination of experimental values from Humbert et al. (Humbert et al., 2011) and our own values (averaged over four experiments) which give access to parameters  $k_{init}$ (eq.10),  $\mu_{CA}$  and  $N_{CA}$  (eq. 8).

Parameters  $\mu_{CA}$  and  $N_{CA}$  have been verified on the unload part of the compressive curves (immediate recovery).

In the second step, the parameters of the plastic deformation ( $\Delta H_{Pl}$  and  $\alpha_{Pl}$ , in equation 9) have been identified on the evolution of the yield point as a function of the strain rate for the weight 10.5 Mg/mol. Here also, the average values based on four experimental tests are used.

In the third step, the strain-hardening of the semicrystalline polymer is determined by a combination of three phenomena:

- The decrease of the intra-cohesive lamellar forces of the crystal network due to the shear of the crystal lamellae and the destruction of the spherulitic structure in favor of a fibrillar structure. In the model proposed here the parameter  $\varepsilon_{Nat\_Crystal}$  (eq.10), corresponding to the deformation for which the fibrillary state is reached, allows to reproduce this decrease.
- The strain hardening due to the entanglement network modeled here by the entropic elasticity decomposed in two parts: the elastic modulus  $C_0$  (parameters  $N_{MN}$  and  $\mu_{MN}$  of the Langevin spring in equation 2) and the dependence with strain rates (parameters  $\Delta H_{MN}$  and  $\alpha_{MN}$  that appears in the expression of  $C_{app}(\dot{\varepsilon})$  in equation 3) combine with the effect of the confined amorphous phase.
- And finally, the disentanglement of the macromolecular chains described by the reptation theory ( $\eta_{flow} = G_{flow} M^3$ ) and the parameters  $\Delta H_{Fibrils}$  and  $\alpha_{Fibrils}$  (eq. 11) describing the slipping of the fibrils.

Consequently, the 7 parameters ( $\varepsilon_{Nat\_Cr}$ ,  $N_{MN}$ ,  $\mu_{MN}$ ,  $\Delta H_{MN}$  and  $\alpha_{MN}$ ,  $\Delta H_{Fibrils}$  and  $\alpha_{Fibrils}$  and  $G_{flow}$ ) have been identified on the evolution of the strain hardening with strain rates and for the molecular weight 10.5 Million g/mol. To obtain the fitting curves of the compressive tests on the material with molecular weights 0.6 and 3.9 Million g/mol only parameters  $\varepsilon_{Nat\_Cr}$ ,  $\Delta H_{MN}$  and  $N_{MN}$  have been numerically identified. All the other parameters are the same as in the case of the molecular mass 10.5 Million g/mol. The complete set of parameters obtained after optimization is given in Table 1.

Several numerical checks were made to verify the consistency of the model: distribution of the strain and stress in the various constituent parts and energy conservation in the system which was verified to be valid in the limit of numerical errors.

#### 4.5. Discussion of the influence of molecular weight and crystallinity on the model parameters

Figure 8 shows the confrontation of the optimized numerical modeling and experimental data of compressive tests for the 3 molecular weights 0.6; 3.9; and 10.5 Million g/mol. This model permits to capture the increase of the ‘strain-hardening modulus’ with the strain-rate and the evolution of the recovery for the three molecular weights.

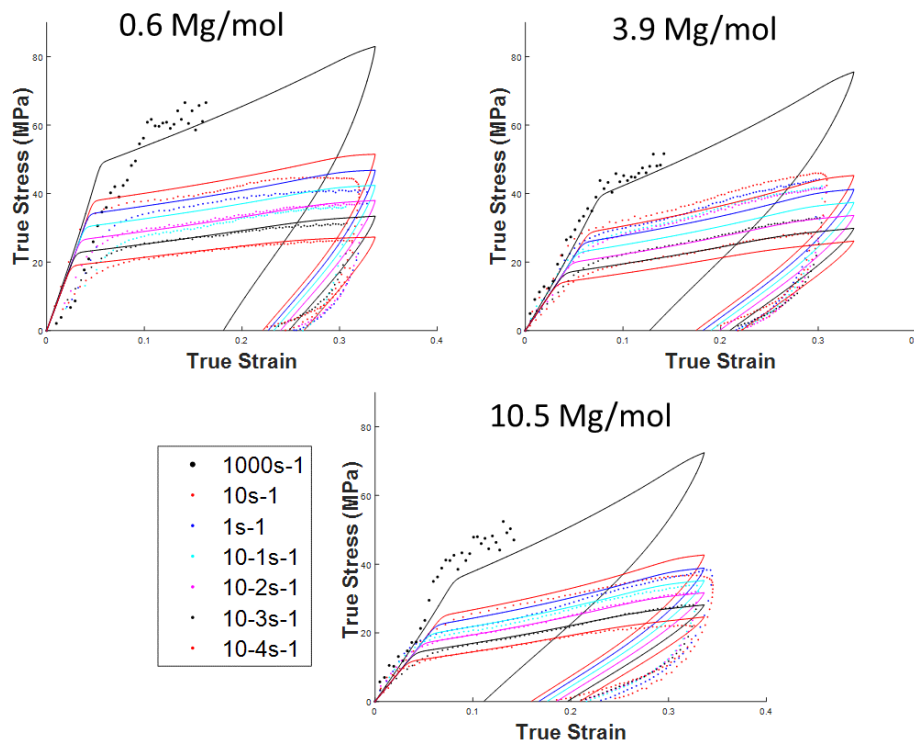


**Figure 8:** Experimental and numerical strain-stress curves for compression test performed on the three molecular weights for various strain rates in the range from  $10^{-4} \text{ s}^{-1}$  to  $1000 \text{ s}^{-1}$ . The

experimental data are given as dot lines and the results of the numerical modeling are continuous lines.

Table 1 presents the set of parameters obtained by the numerical optimization. The first two columns are the molecular weights obtained by viscosity measurement and given by Celanese and the crystallinity of the material measured by DSC. The parameters have been separated in two tables, the first one corresponds to the crystal network and the confined amorphous phase and the second one corresponds to the macromolecular network. It is important to emphasize that the set of parameters are the same for the 3 molecular weights except parameters  $\Delta H_{Pl}$  and  $\varepsilon_{Nat\_Cr}$  associated to the percolation of the crystal network and the role of the tie molecules which vary with the crystallinity, and  $N_{MN}$  representing the number of Kuhn segments between entanglement or cross-linking due to the crystal network (extensibility of the chains in the Boyce model).

Crystalline stacks network								
<b><i>M</i></b> (10 <sup>6</sup> g/mol)	<b><i>φ</i></b> (vol%)	$\alpha_{Pl}$ (10 <sup>-27</sup> m <sup>3</sup> )	$\Delta H_{Pl}$ (10 <sup>-19</sup> J)	$\epsilon_{Nat\_Cr}$	$N_{CA}$	$\mu_{CA}$ (Mpa)	$\alpha_{Fibrils}$ (10 <sup>-27</sup> m <sup>3</sup> )	$\Delta H_{Fibrils}$ (10 <sup>-19</sup> J)
<b>0.6</b>	<b>58</b>	1.65	<b>2</b>	<b>-0.7</b>	1.2	1.8	3.95	1.98
<b>3.9</b>	<b>40</b>	1.65	<b>1.97</b>	<b>-0.8</b>	1.2	1.8	3.95	1.98
<b>10.5</b>	<b>34</b>	1.65	<b>1.93</b>	<b>-0.85</b>	1.2	1.8	3.95	1.98

Macromolecular network						
<b><i>M</i></b> (10 <sup>6</sup> g/mol)	<b><i>φ</i></b> (vol%)	$G_{flow}$ (mol <sup>3</sup> kg <sup>-2</sup> m <sup>-1</sup> s <sup>-1</sup> )	$\alpha_{MN}$ ( $C_{app}(\dot{\epsilon})$ ) (10 <sup>-25</sup> m <sup>3</sup> )	$\Delta H_{MN}$ ( $C_{app}(\dot{\epsilon})$ ) (10 <sup>-20</sup> J)	$\mu_{MN}$ (Mpa)	$N_{MN}$
<b>0.6</b>	<b>58</b>	10 <sup>3</sup>	1.03	9.25	2.4	<b>4.2</b>
<b>3.9</b>	<b>40</b>	10 <sup>3</sup>	1.03	9.25	2.4	<b>3.5</b>
<b>10.5</b>	<b>34</b>	10 <sup>3</sup>	1.03	9.25	2.4	<b>3.5</b>

**Table 1:** Optimized set of parameters of the constitutive model for the crystal network and for the confined amorphous phase (first table) and to the macromolecular network (second table). The first two columns in bold italics are the molecular weights given by the manufacturer, Celanese, and the crystallinity measured by DSC. The two columns in red are the only parameters that change with the molecular weight.

Several verifications of the behavior of the model were made to confirm its consistency with the literature on the mechanical behavior of semicrystalline polymers. For instance, Figure 9 shows the evolution of the yield stress and the apparent natural deformation (corresponding to the deformation for which the fibrillar structure is reached) with the crystallinity. As expected, these two physical parameters increase with the crystallinity. This can be explained by the percolation of the crystal network which improves as the crystallinity increases.

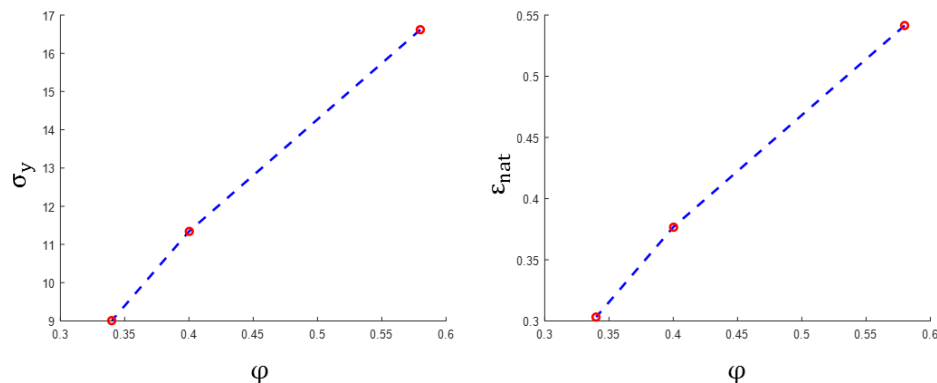


**Figure 9:** Evolution of the yield stress and the apparent natural deformation as a function of the crystallinity obtained by the model.

As explained in the experimental part, the model is developed to reproduce two experimental observations. The first is the unloading part of the curves which remains similar for different deformations. Figure 10 shows the extrapolation of the model to larger deformation and the corresponding experimental behavior for similar strains. One could notice that the unloading part of the curves could be improved. One possible solution would consist in taking into account the chain length distribution. Despite this discrepancy, the overall experimental behavior is nevertheless well captured by the model at least semi-quantitatively.

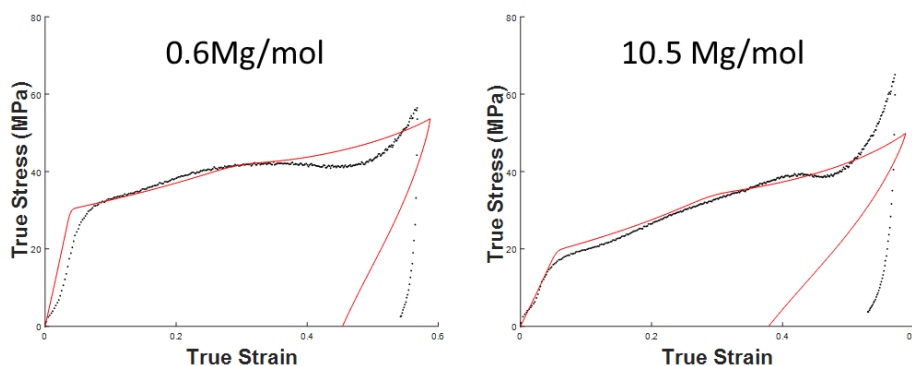


**Figure 10:** Comparison of experimental and numerical stress-strain curves obtained for compression tests performed at  $0.1 \text{ s}^{-1}$  on UHMPE with a molecular weight of (a) 0.6Mg/mol and

(b) 10.5 Mg/mol. The experimental data are given as red-dot lines and the results of the numerical modeling are continuous black lines.

Figure 11 shows the results of an extrapolation of the model to a deformation of 80% for the molecular weights 0.6, 3.9 and 10.5 Mg/mol and strain rates between  $10^{-4} \text{ s}^{-1}$  to  $1000 \text{ s}^{-1}$ .

Here again, the results are in agreement with the experimental observations similarly to what was said regarding Figure 10 for the strain rate  $0.1 \text{ s}^{-1}$ .

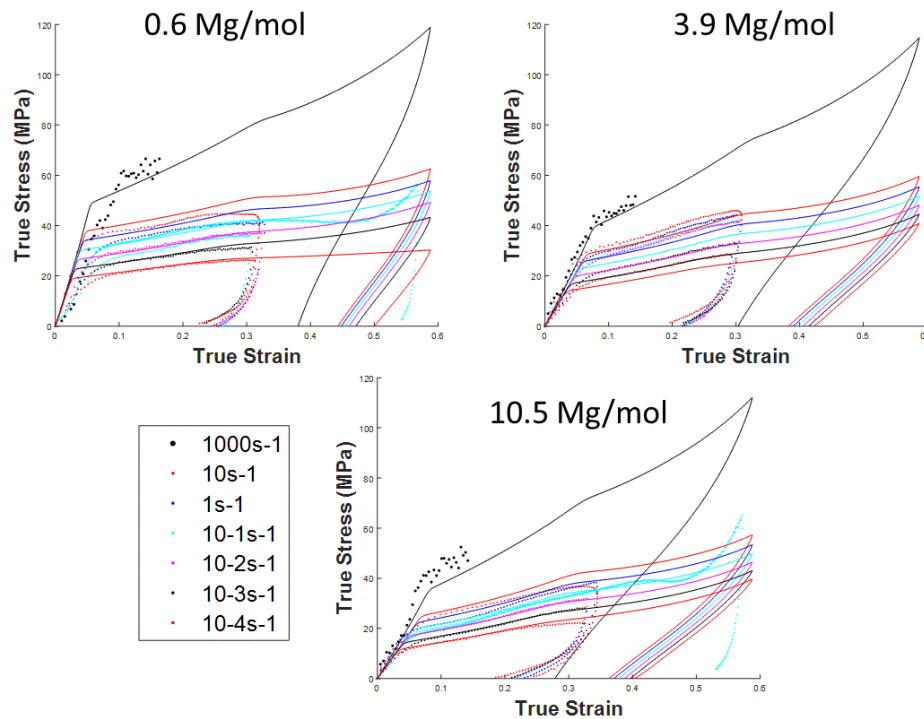


**Figure 11:** Stress-strain curves of the numerical extrapolation of the model to a deformation of 80% for the three molecular weights and various strain rates in the range from  $10^{-4} \text{ s}^{-1}$  to  $1000 \text{ s}^{-1}$ .

Experimental data obtained for lower strain are plotted as dot lines just for the information.

The second experimental observation is a recovery close to 100%, for long time, for the sample with the highest molecular weight. The part representing the macromolecular network allows to

account for this observation since, in the case of this molecular weight, the flow by reptation is nonexistent. Additional experiments, like cyclic tests or relaxation tests, could be done to improve this description.

Finally, Figure 12 shows the extrapolation of the model to a tensile loading condition and the comparison with the experimental data. Interestingly, the model accurately reproduces the mechanical response of these tensile tests and this, without any modification of the model parameters. The dissymmetry contained in the Boyce model appears to be sufficient to take into account the differences between tension and compression.

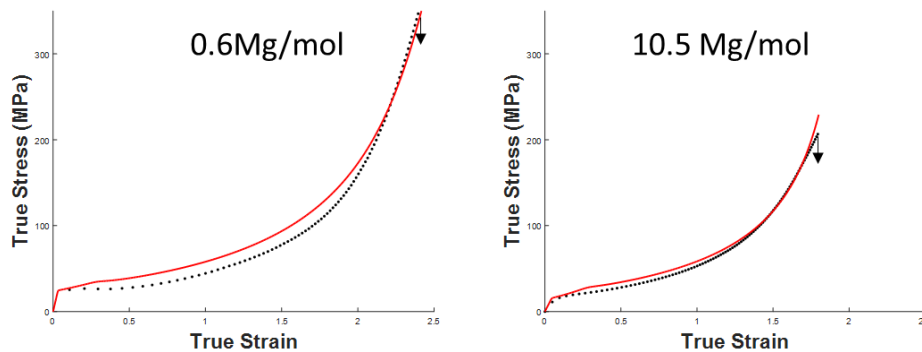


**Figure 12:** Tensile experiments (black dots) and extrapolation of the model (red curves) to tensile loading conditions for the molecular weights 0.6 and 10.5 Mg/mol and at the strain rate  $3.5 \cdot 10^{-3} \text{s}^{-1}$ .

Figure 13 shows an extrapolation of the model to larger deformation and to cyclic loading conditions. These tensile and compressive curves reveal a larger permanent deformation for the lower molecular weight. In other words, the lowest molecular weight accumulates plasticity with the cycles that could potentially lead to failure whereas the cyclic behavior of the highest molecular weight specimen is mostly reversible. This result is in agreement with the differences in cavitation erosion resistance observed for different molecular weights of the UHMWPE (Deplancke et al.,

2015a). This promising typical feature allows to envisage this model for numerical modeling of cavitation erosion where repetitive impacts of multiple bubble collapses need to be taken into account.

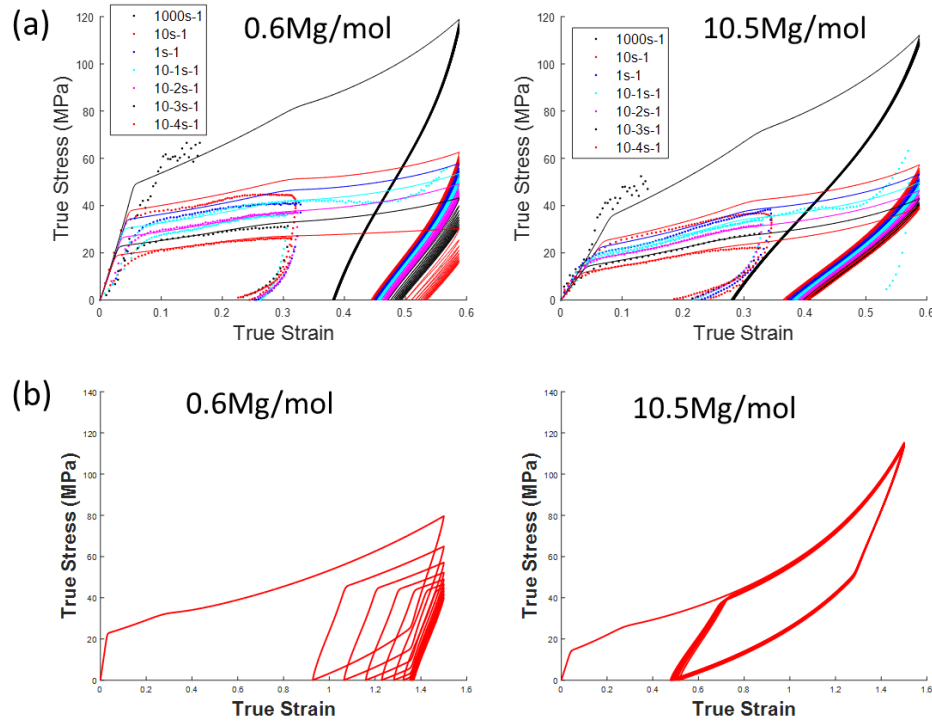


**Figure 13.** Extrapolation of the model for cyclic loading (10 cycles) (a) in compression for different strain rates and (b) in tensile for a strain rate  $0.001 \text{ s}^{-1}$ .

## 5. CONCLUSION

An 1D hyperelastic-viscoplastic constitutive model is proposed to describe the mechanical compressive behavior of semicrystalline polymer with ultra-high molecular weight under a wide range of strain rates. The mechanical behavior of sintered UHMWPE with different molecular weight (0.6; 3.9 and 10.5 Mg/mol) was investigated over a large range of strain rates up to a deformation of 0.4. Experimentally, this range of strain was achieved using uniaxial compression tests performed on a servo-hydraulic testing machine for the lowest strain rates ( $10^{-4}$  to  $10 \text{ s}^{-1}$ )

complemented by magnesium split Hopkinson pressure bar tests for the highest strain rates ( $10^3 \text{ s}^{-1}$ ).

The mechanical behavior is described by a physical approach of the semicrystalline polymers based on a macromolecular network bridled by the crystalline network formed by lamellar stacking. In the case of UHMWPE, the impact of the macromolecular network, both long entangled chains as well as tie molecules, leads to a plastic deformation of the specimen without necking. Indeed, the modulus collapse due to the splintering of the crystalline networks is immediately caught up by the active chains of the macromolecular network.

The originality of the proposed model lies in i) allowing the description of the crystalline network collapse by the decrease along the plastic deformation of the mechanical coupling between rubbery and crystalline phase i.e. the stress transfer to the hard/crystalline phase decreases as the plastic deformation increases, and ii) describing the role of both the confined amorphous phase and the long-entangled chains allowing strain hardening, short and long-term deformation recovery.

After a numerical identification of the twelve parameters of the model, a good agreement was observed between model response and experimental results in a large range of strain rates. Furthermore, the same set of parameters allows to describe 3 different molecular weights (0.6, 3.9 and 10.5 Million g/mol), except two parameters which are logically different since the crystallinity of these materials is different: the percolation of the crystal network and the crystallinity. In addition, due to its physical consistency, the model gives satisfactory qualitative responses both for tensile and cyclic loading conditions largely above the strain range for which the parameters have been adjusted. This confirms that the essential of the physic required to describe the outstanding resistance to cavitation of the UHMWPE is captured by this simple 1D model.

Ongoing work consists of two main actions: (i) investigating other loading conditions such as cyclic loads and (ii) implementation of a 3D version of the model in the finite element code ABAQUS.

## ACKNOWLEDGEMENTS

This research was carried out under project CARAPACE ANR-16-ASTR-0004-04 which provided financial support for Dr. T. Deplancke.

The authors are indebted to Celanese (Oberhausen, Germany) for the generous supply of the UHMWPE sample together with its molecular characteristics. The authors also gratefully acknowledge the support of N. Ranc for the realization of the SHPB tests.

## REFERENCES

- Arruda, E.M., Boyce, M.C., 1993. A three-dimensional constitutive model for the large stretch behavior of rubber elastic materials. *J. Mech. Phys. Solids* 41, 389–412. [https://doi.org/10.1016/0022-5096\(93\)90013-6](https://doi.org/10.1016/0022-5096(93)90013-6)
- Ayoub, G., Zaïri, F., Frédérix, C., Gloaguen, J.M., Naït-abdelaziz, M., Seguela, R., 2011. Effects of crystal content on the mechanical behaviour of polyethylene under finite strains : Experiments and constitutive modeling. *Int. J. Plast.* 27, 492–511. <https://doi.org/10.1016/j.ijplas.2010.07.005>
- Ayoub, G., Zaïri, F., Naït-abdelaziz, M., Gloaguen, J.M., 2010. Modelling large deformation behaviour under loading – unloading of semicrystalline polymers : Application to a high density polyethylene. *Int. J. Plast.* 26, 329–347. <https://doi.org/10.1016/j.ijplas.2009.07.005>
- Bardenhagen, S.G., Stout, M.G., Gray, G.T., 1997. Three-dimensional, finite deformation,

- viscoplastic constitutive models for polymeric materials. *Mech. Mater.* 25, 235–253. [https://doi.org/10.1016/S0167-6636\(97\)00007-0](https://doi.org/10.1016/S0167-6636(97)00007-0)
- Bartczak, Z., Galeski, A., 2010. Plasticity of Semicrystalline Polymers. *Macromol. symp.* 294, 67–90. <https://doi.org/10.1002/masy.201050807>
- Bergström, J.S., Kurtz, S.M., Rimnac, C.M., Edidin, A.A., 2002. Constitutive modeling of ultra-high molecular weight polyethylene under large-deformation and cyclic loading conditions. *Biomaterials* 23, 2329–2343. [https://doi.org/10.1016/S0142-9612\(01\)00367-2](https://doi.org/10.1016/S0142-9612(01)00367-2)
- Bonten, C., Schmachtenberg, E., 2001. A New Hypothesis To Describe the Mechanisms Acting. *Polym. Eng. Sci.* 41, 475–483.
- Bouvard, J.L., Ward, D.K., Hossain, D., Nouranian, S., Marin, E.B., Horstemeyer, M.F., 2009. Review of Hierarchical Multiscale Modeling to Describe the Mechanical Behavior of. *J. Eng. Mater. Technol.* 131. <https://doi.org/10.1115/1.3183779>
- Boyce, M.C., Arruda, E.M., 2000. Constitutive Models of Rubber Elasticity: A Review. *Rubber Chem. Technol.* 73, 504–523. <https://doi.org/10.5254/1.3547602>
- Boyd, R.H., 1979. The modulus of the amorphous component in polyethylenes. *Polym. Eng. Sci.* 19, 1010–1016. <https://doi.org/10.1002/pen.760191408>
- Buckley, C.P., Jones, D.C., 1995. Glass-rubber constitutive model for amorphous polymers near the glass transition. *Polymer (Guildf)*. 36, 3301–3312. [https://doi.org/10.1016/0032-3861\(95\)99429-X](https://doi.org/10.1016/0032-3861(95)99429-X)
- Castagnet, S., Gacougnolle, J.L., Dang, P., 2000. Correlation between macroscopical viscoelastic behaviour and micromechanisms in strained  $\alpha$  polyvinylidene fluoride (PVDF). *Mater. Sci. Eng. A* 276, 152–159. [https://doi.org/10.1016/S0921-5093\(99\)00320-2](https://doi.org/10.1016/S0921-5093(99)00320-2)
- Deplancke, T., Lame, O., Cavaille, J.-Y., Fivel, M., Riondet, M., Franc, J.-P., 2015a. Outstanding

- cavitation erosion resistance of Ultra High Molecular Weight Polyethylene (UHMWPE) coatings. *Wear* 328–329, 301–308. <https://doi.org/10.1016/j.wear.2015.01.077>
- Deplancke, T., Lame, O., Rousset, F., Aguilí, I., Seguela, R., Vigier, G., 2014. Diffusion versus cocrystallization of very long polymer chains at interfaces: Experimental study of sintering of UHMWPE nascent powder. *Macromolecules* 47, 197–207. <https://doi.org/10.1021/ma402012f>
- Deplancke, T., Lame, O., Rousset, F., Seguela, R., Vigier, G., 2015b. Mechanisms of chain reentanglement during the sintering of UHMWPE nascent powder : effect of the molecular weight. *Macromolecules* 48, 5328–5338.
- Detrez, F; Séguéla, R.; Cantournet, S., 2009. Quantification et modelisation du couplage plasticite endommagement dans les polymeres semicristallins a morphologie spherolitique. 19 ème congrès Français Mécanique 1–6.
- Detrez, F., Cantournet, S., Seguela, R., 2011. Plasticity / damage coupling in semi-crystalline polymers prior to yielding : Micromechanisms and damage law identification. *Polymer (Guildf)*. 52, 1998–2008. <https://doi.org/10.1016/j.polymer.2011.03.012>
- Doi, M., Edwards, S.F., 1988. *The theory of polymer dynamics*, Oxford uni. ed.
- Dommelen, J.A.W. Van, Parks, D.M., Boyce, M.C., 2003. Micromechanical modeling of the elasto-viscoplastic behavior of semi-crystalline polymers. *J. Mech. Phys. Solids* 51, 519–541.
- Drozdov, A.D., 2009. Mullins' effect in semicrystalline polymers: Experiments and modeling. *Int. J. Solids Struct.* 46, 3336–3345. <https://doi.org/10.1007/s11012-010-9314-z>
- Dusunceli, N., Colak, O.U., 2008. Modelling effects of degree of crystallinity on mechanical behavior of semicrystalline polymers. *Int. J. Plast.* 24, 1224–1242. <https://doi.org/10.1016/j.ijplas.2007.09.003>

- Epee, A.F., Lauro, F., Bennani, B., Bourel, B., 2011. Constitutive model for a semi-crystalline polymer under dynamic loading. *Int. J. Solids Struct.* 48, 1590–1599. <https://doi.org/10.1016/j.ijsolstr.2011.02.009>
- Eyring, H., 1936. Viscosity, Plasticity, and Diffusion as Examples of Absolute Reaction Rates. *J. Chem. Phys.* 4, 283–291. <https://doi.org/10.1063/1.1749836>
- G'sell, C., Dahoun, A., 1994. Evolution of microstructure in semi-crystalline polymers under large plastic deformation. *Mater. Sci. Eng. A* 175, 183–199. [https://doi.org/10.1016/0921-5093\(94\)91058-8](https://doi.org/10.1016/0921-5093(94)91058-8)
- Gama, B.A., Lopatnikov, S.L., Gillespie, J.W., 2004. Hopkinson bar experimental technique: A critical review. *Appl. Mech. Rev.* 57, 223. <https://doi.org/10.1115/1.1704626>
- Gent, A.N., Madan, S., 1989. Plastic Yielding of Partially Crystalline Polymers. *J. Polym. Sci. Part B Polym. Phys.* 27, 1529–1542.
- Goveart, L.E., Engels, T.A.P., Wendlandt, M., Tervoort, T.A., Suter, U.W., 2008. Does the Strain Hardening Modulus of Glassy Polymers Scale with the Flow Stress? *Polym. Eng. Sci.* 46, 2175–2481. <https://doi.org/10.1002/polb>
- Gueguen, O., Ahzi, S., Makradi, A., Belouettar, S., 2010. Mechanics of Materials A new three-phase model to estimate the effective elastic properties of semi-crystalline polymers: Application to PET. *Mech. Mater.* 42, 1–10. <https://doi.org/10.1016/j.mechmat.2009.04.012>
- Gueguen, O., Richeton, J., Ahzi, S., Makradi, A., 2008. Micromechanically based formulation of the cooperative model for the yield behavior of semi-crystalline polymers. *Acta Mater.* 56, 1650–1655. <https://doi.org/10.1016/j.actamat.2007.12.015>
- Halpin, J.C., Kardos, J.L., 1976. The Halpin-Tsai equations: A review. *Polym. Eng. Sci.* 16, 344–352. <https://doi.org/10.1002/pen.760160512>

- Haward, R.N., 1993. Strain-hardening thermoplastic. *Macromolecules* 26, 5860–5869.
- Haward, R.N., Thackray, G., 1968. The Use of a Mathematical Model to Describe Isothermal Stress-Strain Curves in Glassy Thermoplastics. *Proc. R. Soc. A Math. Phys. Eng. Sci.* 302, 453–472. <https://doi.org/10.1098/rspa.1968.0029>
- Huang, Y. -L, Brown, N., 1991. Dependence of slow crack growth in polyethylene on butyl branch density: Morphology and theory. *J. Polym. Sci. Part B Polym. Phys.* 29, 129–137. <https://doi.org/10.1002/polb.1991.090290116>
- Humbert, S., Lame, O., Séguéla, R., Vigier, G., 2011. A re-examination of the elastic modulus dependence on crystallinity in semi-crystalline polymers. *Polymer (Guildf)*. 52, 4899–4909. <https://doi.org/10.1016/j.polymer.2011.07.060>
- Humbert, S., Lame, O., Vigier, G., 2009. Polyethylene yielding behaviour: What is behind the correlation between yield stress and crystallinity? *Polymer (Guildf)*. 50, 3755–3761. <https://doi.org/10.1016/j.polymer.2009.05.017>
- Khan, A., Zhang, H., 2001. Finite deformation of a polymer: Experiments and modeling. *Int. J. Plast.* 17, 1167–1188. [https://doi.org/10.1016/S0749-6419\(00\)00073-5](https://doi.org/10.1016/S0749-6419(00)00073-5)
- Khan, A.S., Lopez-pamies, O., Kazmi, R., 2006. Thermo-mechanical large deformation response and constitutive modeling of viscoelastic polymers over a wide range of strain rates and temperatures. *Int. J. Mech. Sci.* 22, 581–601. <https://doi.org/10.1016/j.ijplas.2005.08.001>
- Krairi, A., Doghri, I., 2014. A thermodynamically-based constitutive model for thermoplastic polymers coupling viscoelasticity, viscoplasticity and ductile damage. *Int. J. Plast.* 60, 163–181. <https://doi.org/10.1016/j.ijplas.2014.04.010>
- Lee, B., Parks, D.M., Ahzi, S., 1993. Micromechanical modeling of large plastic deformation and texture evolution in semi-crystalline polymers. *J. Mech. Phys. Solids* 41, 1651–1687.

[https://doi.org/10.1016/0022-5096\(93\)90018-B](https://doi.org/10.1016/0022-5096(93)90018-B)

- Maurel-Pantel, A., Baquet, E., Bikard, J., Bouvard, J.L., Billon, N., 2015. A thermo-mechanical large deformation constitutive model for polymers based on material network description: Application to a semi-crystalline polyamide 66. *Int. J. Plast.* 67, 102–126. <https://doi.org/10.1016/j.ijplas.2014.10.004>
- Men, Y., Rieger, J., Strobl, G., 2003. Role of the Entangled Amorphous Network in Tensile Deformation of Semicrystalline Polymers. *Phys. Rev. Lett.* 91, 095502. <https://doi.org/10.1103/PhysRevLett.91.095502>
- Michler, G.H., Baltá-Calleja, F.J., 2016. *Mechanical Properties of Polymers based on Nanostructure and Morphology*, CRC Press. ed.
- Nikolov, S., Doghri, I., Pierard, O., Zealouk, L., Goldberg, A., 2002. Multi-scale constitutive modeling of the small deformations of semi-crystalline polymers. *J. Mech. Phys. Solids* 50, 2275–2302. [https://doi.org/10.1016/S0022-5096\(02\)00036-4](https://doi.org/10.1016/S0022-5096(02)00036-4)
- Oshmyan, V., Patlazhan, S., Remond, Y., 2004. Simulation of small-strain deformations of semi-crystalline polymer: Coupling of structural transformations with stress-strain response. *J. Mater. Sci.* 39, 3577–3586. <https://doi.org/10.1023/B:JMSC.0000030709.19754.28>
- Patel, R.M., Sehanobish, K., Jain, P., Chum, S.P., Knight, G.W., 1996. Theoretical prediction of tie-chain concentration and its characterization using postyield response. *J. Appl. Polym. Sci.* 60, 749–758.
- Peterlin, A., 1987. Drawing and extrusion of semi-crystalline polymers. *Colloid Polym. Sci.* 265, 357–382. <https://doi.org/10.1007/BF01412215>
- Peterlin, A., 1975. Plastic deformation of polymers with fibrous structure. *Colloid Polym. Sci.* 253, 809–823.

- Peterlin, A., 1967. Folded chain concept of fiber structure. *Colloid Polym. Sci.* 216, 129–136.
- Pfeiffer, R., 2015. Analyse et modélisation du fraisage du bois vert. *École Nationale Supérieure d'Arts et Métiers*.
- Porter, R.S., Johnson, J.F., 1966. The entanglement concept in polymer systems. *Chem. Rev.* 66.
- Pouriayevali, H., Arabnejad, S., Guo, Y.B., Shim, V.P.W., 2013. A constitutive description of the rate-sensitive response of semi-crystalline polymers. *Int. J. Impact Eng.* 62, 35–47. <https://doi.org/10.1016/j.ijimpeng.2013.05.002>
- Regrain, C., Laiarinandrasana, L., Toillon, S., Sai, K., 2009. Multi-mechanism models for semi-crystalline polymer: Constitutive relations and finite element implementation. *Int. J. Plast.* 25, 1253–1279. <https://doi.org/10.1016/j.ijplas.2008.09.010>
- Richeton, J., Ahzi, S., Daridon, L., Rémond, Y., 2005. A formulation of the cooperative model for the yield stress of amorphous polymers for a wide range of strain rates and temperatures. *Polymer (Guildf)*. 46, 6035–6043. <https://doi.org/10.1016/j.polymer.2005.05.079>
- Roguet, E., Castagnet, S., Grandidier, J.C., 2007. Mechanical features of the rubbery amorphous phase in tension and torsion in a semi-crystalline polymer. *Mech. Mater.* 39, 380–391. <https://doi.org/10.1016/j.mechmat.2006.06.003>
- Roy, S.C., Franc, J.P., Pellone, C., Fivel, M., 2015. Determination of cavitation load spectra - Part 1: Static finite element approach. *Wear* 344–345, 110–119. <https://doi.org/10.1016/j.wear.2015.09.006>
- Sedighiamiri, A., Senden, D.J.A., Tranchida, D., Govaert, L.E., Dommelen, J.A.W. Van, 2014. A micromechanical study on the deformation kinetics of oriented semicrystalline polymers. *Comput. Mater. Sci.* 82, 415–426. <https://doi.org/10.1016/j.commatsci.2013.09.068>
- Seguela, R., 2007. On the Natural Draw Ratio of Semi-Crystalline Polymers: Review of the

- Mechanical, Physical and Molecular Aspects. *Macromol. Mater. Eng.* 292, 235–244.  
<https://doi.org/10.1002/mame.200600389>
- Seguela, R., 2005. Critical review of the molecular topology of semicrystalline polymers: The origin and assessment of intercrystalline tie molecules and chain entanglements. *J. Polym. Sci. Part B Polym. Phys.* 43, 1729–1748. <https://doi.org/10.1002/polb.20414>
- Senden, D.J.A., Van Dommelen, J.A.W., Goveart, L.E., 2010. Strain Hardening and its Relation to Bauschinger Effects in Oriented Polymers. *J. Polym. Sci. Part B Polym. Phys.* 48, 1483–1494. <https://doi.org/10.1002/polb>
- Shojaei, A., Li, G., 2013. Viscoplasticity analysis of semicrystalline polymers: A multiscale approach within micromechanics framework. *Int. J. Plast.* 42, 31–49.  
<https://doi.org/10.1016/j.ijplas.2012.09.014>
- Tarin, P.M., Thomas, E.L., 1979. The role of inter- and intra-links in the transformation of folded chain lamellae into microfibrils. *Polym. Eng. Sci.* 19, 1017–1022.  
<https://doi.org/10.1002/pen.760191409>
- Uchida, M., Tokuda, T., Tada, N., 2010. Finite element simulation of deformation behavior of semi-crystalline polymers with multi-spherulitic mesostructure. *Int. J. Mech. Sci.* 52, 158–167. <https://doi.org/10.1016/j.ijmecsci.2009.09.002>
- Wang, J., Porter, R.S., 1995. On the viscosity-temperature behavior of polymer melts. *Rheol. Acta* 34, 496–503. <https://doi.org/10.1007/BF00396562>
- Ward, I.M., 1984. The Role of Molecular Networks and Thermally Activated Processes in the Deformation-Behavior of Polymers. *Polym. Eng. Sci.* 24, 724–736. <https://doi.org/DOI.10.1002/pen.760241003>
- Ward, I.M., Sweeney, J., 2001. *The mechanical properties of solid polymers*, Wiley. ed.

[https://doi.org/10.1002/1521-3773\(20010316\)40:6<9823::AID-ANIE9823>3.3.CO;2-C](https://doi.org/10.1002/1521-3773(20010316)40:6<9823::AID-ANIE9823>3.3.CO;2-C)

Wunderlich, B., 2003. *Macromolecular Physics*.

Xiong, B., Lame, O., Chenal, J.M., Rochas, C., Seguela, R., 2016. On the strain-induced fibrillar microstructure of polyethylene: Influence of chemical structure, initial morphology and draw temperature. *Express Polym. Lett.* 10, 311–323.  
<https://doi.org/10.3144/expresspolymlett.2016.29>

Xiong, B., Lame, O., Chenal, J.M., Rochas, C., Seguela, R., Vigier, G., 2015. Amorphous phase modulus and micro-macro scale relationship in polyethylene via in situ SAXS and WAXS. *Macromolecules* 48, 2149–2160. <https://doi.org/10.1021/acs.macromol.5b00181>

Xue, Y., Tervoort, T.A., Lemstra, P.J., 1998. Welding Behavior of Semicrystalline Polymers . 1 . The Effect of Nonequilibrium Chain Conformations on Autoadhesion of UHMWPE. *Macromolecules* 31, 3075–3080.

Yakimets, I., Lai, D., Guigon, M., 2007. Model to predict the viscoelastic response of a semi-crystalline polymer under complex cyclic mechanical loading and unloading conditions. *Mech. Time-Dependent Mater.* 11, 47–60. <https://doi.org/10.1007/s11043-007-9031-8>